Stability of liquid bridges subject to an eccentric rotation

V. Lapuerta , A. Laverón-Simavilla, J. Rodríguez

E.T.S.I. Aeronáuticos (Universidad Politécnica de Madrid), Plaza de Cardenal Cisneros, 3, 28040 Madrid, Spain

Abstract

A cylindrical liquid bridge supported between two circular-shaped disks in isorotation is considered. The effect of an offset between the rotation axis and the axis of the two supporting disks (eccentricity) on the stability of the static liquid bridge is investigated. A numerical method is used to find stable and unstable shapes and to determine the stability limit for different values of eccentricity. The calculated stability limits are compared with analytical results, recovering the same behavior. Numerical results have been also compared with the results of an experiment aboard TEXUS-23, recovering the stability limit and the equilibrium shapes.

Keywords: Liquid bridge; Microgravity; Stability

1. Introduction

The behavior of liquid bridges has been widely studied, both theoretically and experimentally, due to the use of this configuration in a crystal growth technique known as the floating zone technique (Meseguer and Sanz, 1985). In this technique, rotation of the supports is used to achieve a uniform temperature field.

In this paper a cylindrical liquid bridge supported between two circular-shaped disks in isorotation is considered. In the absence of gravity, two types of instability, namely, C-mode and amphora mode, depending on the slenderness, can appear (Vega and Perales, 1983; Perales et al., 1990). The effect of an offset between the rotation axis and the axis of the two supporting disks (eccentricity) on these stabilities is investigated.

The stability limits and the equilibrium shapes of the configuration are calculated using an extension of an already implemented numerical method (Laverón-Simavilla and Perales, 1995; Laverón-Simavilla and Checa, 1997).

The calculated stability limits are compared with the analytical results of Perales et al. (1990) (only valid for small eccentricity). The numerical method is used to find stable and unstable shapes and to determine the stability limit for different values of eccentricity, not only restricted to small eccentricity.

For the C-mode, numerical results have been also compared with the results of an experiment aboard TEXUS-23 (see Sanz et al. (1992)) recovering the stability limit and the equilibrium shapes.

2. Problem formulation

The fluid configuration consists of a liquid bridge as sketched in Fig. 1: the liquid column is held by surface tension forces between two disks of radius R_0, placed a distance L apart. Both disks are parallel and coaxial. The volume of the bridge is that corresponding to a cylindrical one: $V = \pi R_0^2 L$. The liquid and the disks are solidly rotating at an angular speed Ω around an axis which is parallel to the axis of the disks, and is placed a small distance E (eccentricity) apart from this line.

The equation governing the steady shape of the liquid bridge is obtained by expressing the equilibrium between the different forces at the interface

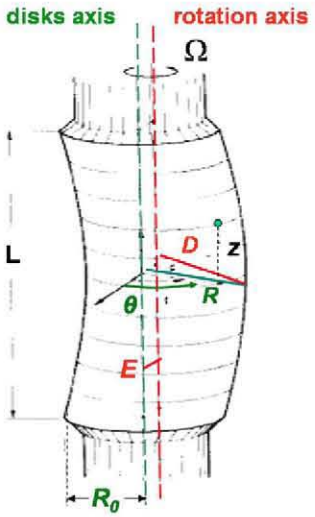

Fig. 1. Geometry and coordinate system for the liquid bridge problem.

$$\sigma\tilde{M}(R)+\tilde{P}+\frac{1}{2}\rho\Omega^2D^2=0 \tag{1}$$

where $R=R(Z,\theta)$ is equation of the gas–liquid interface, σ is the surface tension, $\tilde{M}(R)$ is twice the mean curvature of the interface, $\tilde{P}$ is the pressure difference at the origin, ρ is the liquid density, Ω is the angular speed and D is the distance between a point of the free surface and the rotation axis (see Fig. 1) which, in terms of the shape of the surface and the azimuthal angle θ, can be calculated as:

$$D=(R^2+2ER\cos\theta+E^2)^{1/2} \tag{2}$$

Eq. (1) has to be integrated with the boundary conditions

$$R(\pm L/2,\theta)=R_0 \tag{3}$$

$$R(Z,\theta)=R(Z,\theta+2\pi) \tag{4}$$

$$\frac{1}{2}\int_{-L/2}^{L/2}\mathrm{d}Z\int_0^{2\pi}R^2(Z,\theta)\,\mathrm{d}\theta=\pi LR_0^2 \tag{5}$$

Eq. (3) indicates that the liquid column remains anchored to the disk edges, Eq. (4) comes from the azimuthal periodicity and Eq. (5) expresses the conservation of the volume of the liquid bridge.

Let us introduce the following dimensionless variables and parameters:

$$\Lambda=L/2R_0,\quad e=E/R_0,\quad W=\rho\Omega^2R_0^3/\sigma,$$
$$P=\tilde{P}R_0/\sigma,\quad z=Z/R_0,\quad F(z,\theta)=R(z,\theta)/R_0 \tag{6}$$

where Λ is the liquid bridge slenderness, e is the dimensionless eccentricity, W is the Weber number and P is the dimensionless reference pressure.

The formulation of the problem becomes

$$M(F)+P+\frac{1}{2}W(F^2+2eF\cos\theta+e^2)=0 \tag{7}$$

with

$$M(F)=\frac{F(1+F_z^2)(F_{\theta\theta}-F)+FF_{zz}(F^2+F_\theta^2)-2F_\theta(F_\theta+FF_zF_{\theta\theta})}{(F^2(1+F_z^2)+F_\theta^2)^{3/2}} \tag{8}$$

The dimensionless boundary conditions for Eq. (7) are

$$F(\pm\Lambda,\theta)=1 \tag{9}$$

$$F(z,\theta)=F(z,\theta+2\pi) \tag{10}$$

$$\int_{-\Lambda}^{\Lambda}\mathrm{d}z\int_0^{2\pi}F^2(z,\theta)\,\mathrm{d}\theta=4\pi\Lambda \tag{11}$$

3. Numerical method

An algorithm, based on a continuation method (Keller, 1987) capable of overpassing bifurcation points and turning points (which appear for the amphora mode and the C-mode, respectively) was developed using a finite difference method (Laverón-Simavilla and Perales, 1995) and was used to obtain the bifurcation diagrams and equilibrium shapes of liquid bridges subjected to lateral acceleration and other effects. The stable or unstable character of each of the shapes is calculated to determine the position of the stability limit.

In this paper the system of Eqs. (7)–(11) is solved by using an extension of that algorithm to liquid bridges rotating around an eccentric axis to study the effect of combined eccentricity and angular speed.

The method is based on linearizing Eqs. (7)–(11) around a known solution $(F_0(z,\theta),\ P_0)$ by seeking solutions of the form

$$F(z,\theta)=F_0(z,\theta)+f(z,\theta)+\mathrm{o}(|f|)$$
$$P=P_0+p+\mathrm{o}(|p|)$$

where $|f/F_0|\ll 1$ and $|p/P_0|\ll 1$, and the character 'o' means that the terms not considered are very small compared to the smallest one retained. The leading terms obtained from Eq. (7) result in an equation for $f(z,\theta)$

$$\begin{aligned}\tilde{O}^{-3/2}&\left\{\tilde{A}+\left(\tilde{B}-\frac{3\tilde{A}\tilde{Q}}{2\tilde{O}}\right)f+\left(\tilde{C}-\frac{3\tilde{A}\tilde{S}}{2\tilde{O}}\right)f_z+\left(\tilde{D}-\frac{3\tilde{A}\tilde{T}}{2\tilde{O}}\right)f_\theta\right\}\\&+\tilde{E}f_{zz}+\tilde{G}f_{\theta\theta}+\tilde{H}f_{z\theta}+P_0+p+\frac{1}{2}W\left(e^2+F_0^2+2F_0f\right)\\&+eW(F_0+f)\cos\theta+\frac{1}{2}We^2=0\end{aligned} \tag{12}$$

where $\tilde{A},\tilde{B},\tilde{C},\tilde{D},\tilde{E},\tilde{G},\tilde{H},\tilde{O},\tilde{Q},\tilde{S}$ and $\tilde{T}$ are known functions of $F_0(z,\theta)$ and P_0 and consequently of the considered point on the interface. The leading terms obtained for the boundary conditions are

$$f(z,\theta)=f(z,\theta+2\pi) \tag{13}$$

$$F_0(\pm\Lambda,\theta)+f(\pm\Lambda,\theta)=0 \tag{14}$$

$$\int_{-\Lambda}^{\Lambda}\mathrm{d}z\int_0^{2\pi}F_0(z,\theta)^2\,\mathrm{d}\theta+2\int_{-\Lambda}^{\Lambda}\mathrm{d}z\int_0^{2\pi}[F_0(z,\theta)f(z,\theta)]\,\mathrm{d}\theta=4\pi\Lambda \tag{15}$$

If $(F_0(z,\theta),\ P_0)$ is an exact solution of the problem, Eqs. (12)–(15) can be simplified, but all the terms have been retained because $(F_0(z,\theta),\ P_0)$ will only be an approximation to the solution in the iterative scheme here applied.

The iterative scheme is started from a known solution $(F_0, P_0, \Lambda, W=0,\ e=0)$, the solution is introduced in Eqs. (19)–(23) increasing the value of the Weber number by a small amount $(W=W_1)$, and the linear terms (f,p) are calculated. The new values $(F_0=F_0+f,\ P_0=P_0+p,\ \Lambda,\ W=W_1,\ e=0)$ are introduced again in Eqs. (19)–(23) to get a new set for (f,p), and the procedure is repeated until $\|f\|^2+p^2\leqslant 10^{-6}$ and the equilibrium shape is finally obtained $(F_1=F_0+f,\ P_1=P_0+p,\ \Lambda,\ W=W_1,\ e=0)$. The iteration starts again with an increased value of the Weber number $(W=W_2)$ to get a new equilibrium shape $(F_2=F_0+f, P_2=P_0+p, \Lambda, W=W_2, e=0)$. All the equilibrium shapes obtained are stored to be used as initial forms for an iterative scheme identical to the one described but increasing the value of the eccentricity, e, until the bifurcation diagram is completed.

In order to develop a center finite difference scheme the domain has been characterized by a mesh, defined as the intersection of the free surface with the following planes:

$$z=\Lambda\left(\frac{2j}{J}-1\right),\quad j=0,1,\ldots,J \tag{16}$$

$$\theta=\frac{2\pi}{I+1}i,\quad i=0,1,\ldots,I \tag{17}$$

By doing so, the system (12)–(15) yield a linearized finite difference equation system which can be written as follows:

$$\begin{aligned}&\alpha_{ij}f_j^i+\beta_{ij}f_{j-1}^i+\gamma_{ij}f_{j+1}^i+\delta_{ij}f_j^{i-1}+\varphi_{ij}f_j^{i+1}\\&\quad+\phi_{ij}(f_{j+1}^{i+1}-f_{j+1}^{i-1}-f_{j-1}^{i+1}+f_{j-1}^{i-1})+p\\&\quad=\psi_{ij},\quad i=0,\ldots,I,\ j=0,\ldots,J\end{aligned} \tag{18}$$

$$f_j^0-f_j^{I+1}=0 \tag{19}$$

$$f_J^i=1-F_{0,J}^i,\quad i=0,\ldots,I \tag{20}$$

$$f_0^i=1-F_{0,0}^i,\quad i=0,\ldots,I \tag{21}$$

$$\sum_{i=0}^{I}\sum_{j=0}^{J}a_{ij}f_j^i=A \tag{22}$$

where the coefficients α_{ij}, β_{ij}, γ_{ij}, δ_{ij}, φ_{ij}, ϕ_{ij}, ψ_{ij}, a_{ij} and A are functions of the values $F_{0,j}^i$ and P_0.

If no further modifications were made, the algorithm would destabilize when crossing any critical point. To stabilize the algorithm a new equation defining the arc-length parameter needs to be included. The details of the numerical method used to locate bifurcation and limit points are identical to those outlined elsewhere (Laverón-Simavilla and Perales, 1995) and will not be repeated here. In that paper an analysis of the errors of the numerical method was made finding that a minimum number of points in the mesh is needed to be able to find the complete bifurcation diagram, and this minimum increases as the slenderness of the liquid bridge decreases. The size of the mesh chosen to obtain the results presented in this paper is $I\times J=19\times 28$.

4. Results

First, let us summarize the analytical results of Perales et al. (1990) (only valid for small eccentricity). They looked for a solution of Eqs. (7)–(11) for $e=0$ of the form: $F=1+\varepsilon f+\mathrm{o}(\varepsilon)$, $P=1-W/2+\varepsilon p+\mathrm{o}(\varepsilon)$, $\varepsilon\ll 1$ (small departures from a cylindrical liquid bridge), finding the non-zero solutions:

(i) Non-axisymmetric shapes (C-mode)

$$W_0=\left(\frac{\pi}{2\Lambda}\right)^2,\quad f=\cos\theta\cos\left(\frac{\pi}{2\Lambda}z\right),\quad p=0 \tag{23}$$

(ii) Axisymmetric shapes (amphora mode)

$$W_0=\left(\frac{\pi}{\Lambda}\right)^2-1,\quad f=\sin\left(\frac{\pi}{\Lambda}z\right),\quad p=0 \tag{24}$$

The functions $W_0(\Lambda)$ represent in the Λ–W plane the curves where the transition between stable and unstable equilibrium shapes appears. These two curves have been plotted in Fig. 2. The bifurcation diagrams are as the ones sketched in Figs. 3 and 4 for $e=0$, that is, the bifurcation is

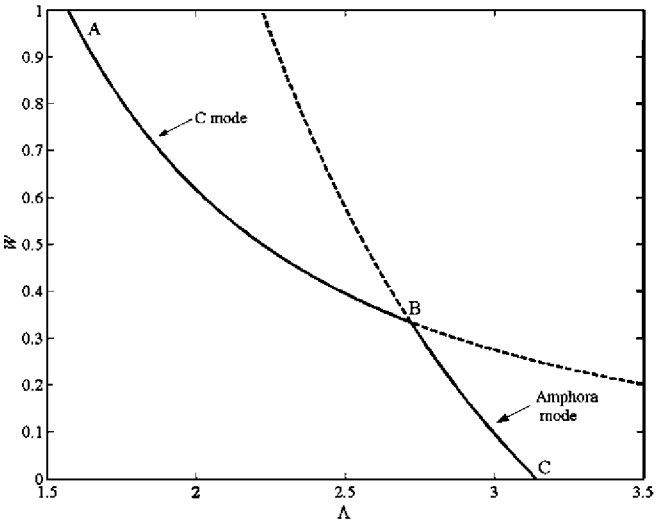

Fig. 2. Stability diagram without eccentricity. Curve AB represents loss of stability with non-axisymmetric breakage and curve BC with axisymmetric breakage.

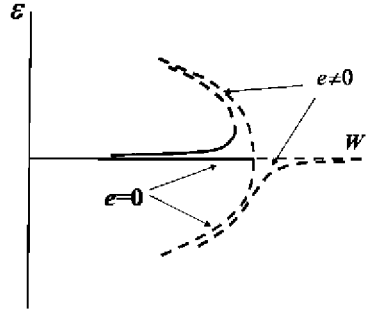

Fig. 3. Bifurcation diagram for the C-mode.

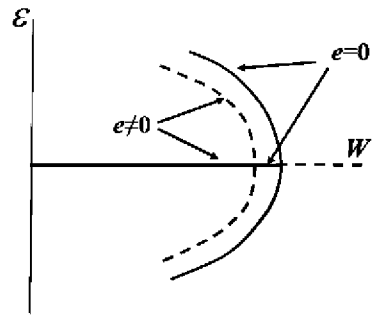

Fig. 4. Bifurcation diagram for the amphora mode.

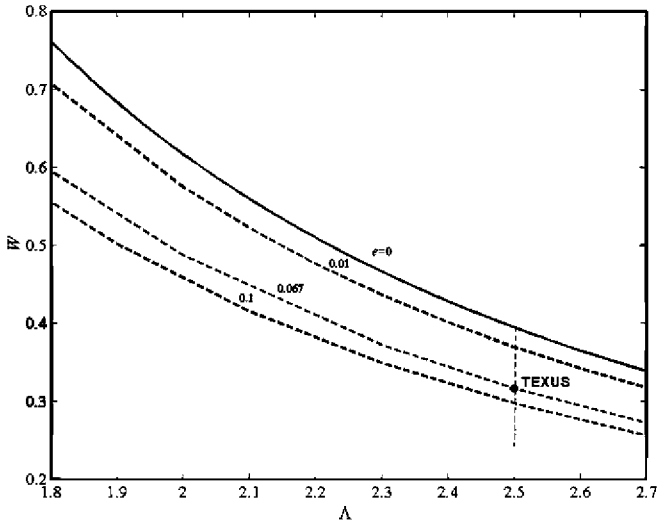

Fig. 5. Effect of the eccentricity on the threshold stability for C-mode.

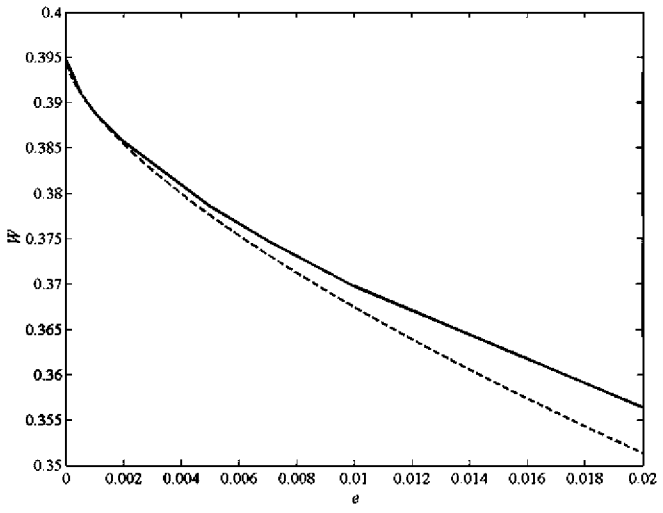

Fig. 6. Comparison of numerical (solid line) and analytical results (dashed line) for C-mode ($\Lambda = 2.5$).

subcritical. Thus, both equilibrium shapes (C-mode shapes and amphora mode shapes) are always unstable. Then, if the rotation speed is slowly increased from zero, one has stable cylindrical shapes until W reaches W_0 at which point the solution becomes unstable.

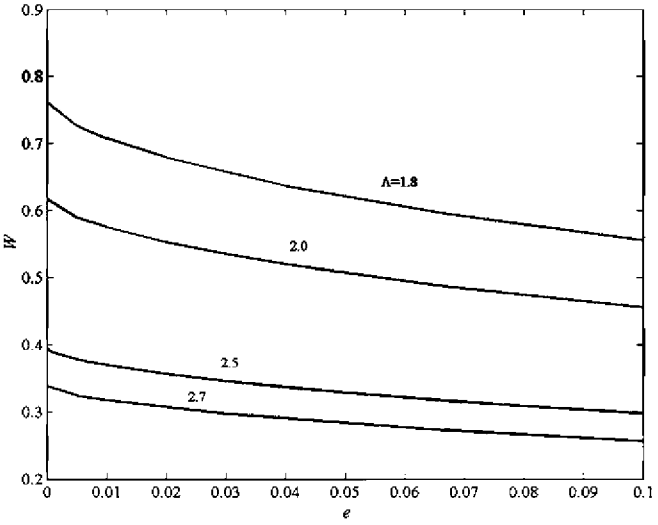

Fig. 7. Effect of the slenderness on the threshold stability.

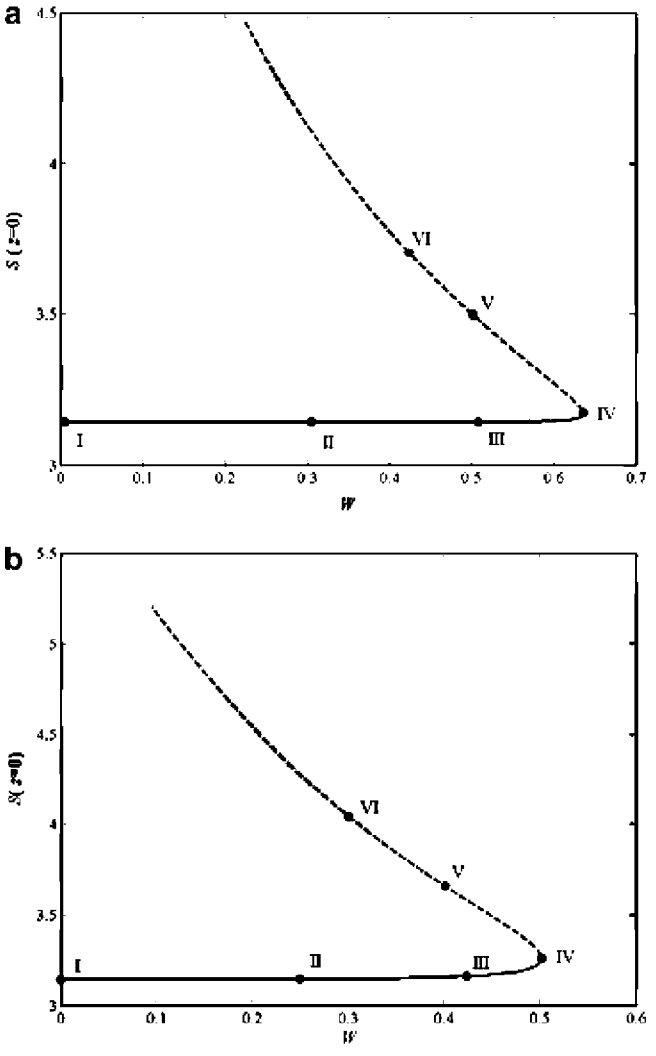

Fig. 8. Bifurcation diagram for the C-mode with $\Lambda = 1.9$ and (a) $e = 0.01$, (b) $e = 0.1$.

Next, we analyze the influence of combined eccentricity and angular speed for both C and amphora modes.

4.1. C-mode

In the following liquid bridges with $\Lambda < \sqrt{3}\pi/2$ are analyzed. For this case the bifurcation equation obtained from the analytical model with $e \ll 1$ takes the form

$$W = W_0 + 3\phi_{300}^{1/3}(\Lambda)\left(\frac{\pi}{2\Lambda^2}\right)^{2/3} e^{2/3} + \cdots \tag{25}$$

where $W_0(\Lambda)$ is given by Eq. (24) and $\phi_{300} < 0$ is given in Perales et al. (1990). This relationship has been sketched in Fig. 3. The effect of the eccentricity for C-mode changes the character of the destabilization, because it is due to a turning point (for $e \neq 0$) instead of a subcritical bifurcation point (for $e = 0$).

With the numerical method we have recovered the stability threshold for $e = 0$, and we have analyzed the dependence of this threshold on the eccentricity and the angular speed. Fig. 5 shows the variation of the stability threshold for increasing eccentricity. The line for $e = 0$ corresponds to the threshold represented in Fig. 2. As we can see in Fig. 5 an increase of the eccentricity decreases the stability region.

Fig. 6 compares the variation of W with e for both numerical and analytical results from Eq. (26) for $\Lambda = 2.5$ (indicated with a vertical dashed line in Fig. 5). These results agree very well for $e \ll 1$ and the disagreement increases as the eccentricity increases, as expected, because the analytical results were developed for $e \ll 1$. The evolution of W with e for different values of Λ is shown in Fig. 7. As we can see in this figure, the effect of slenderness in the stability is similar to that for $e = 0$, that is, an increase of Λ decreases the stability region.

Next we show the main branch of the bifurcation diagram, obtained by representing the area of the section at $z = 0$ as a function of W, and the equilibrium shapes for two different values of the eccentricity.

(a) $\Lambda = 1.9$, $e = 0.01$. Fig. 8(a) shows the bifurcation diagram. The stable part of the branch is represented with a solid line, and the unstable part, after overpassing the turning point, with a dashed line.

(b) $\Lambda = 1.9$, $e = 0.1$. Fig. 8(b) shows the bifurcation diagram. Equilibrium shapes for points I to VI marked in Fig. 8(b) are represented in Fig. 9.

In both cases the shapes obtained are symmetric about the $z = 0$ plane and present two necks that become narrower as e evolves.

4.2. Amphora mode

In the following liquid bridges with $\Lambda > \sqrt{3}\pi/2$ are analyzed. For this case the bifurcation equation obtained from the analytical model with $e \ll 1$ takes the form

$$W = W_0(\Lambda) - \frac{\phi_{120}}{\phi_{101}} e^2 + \cdots \tag{26}$$

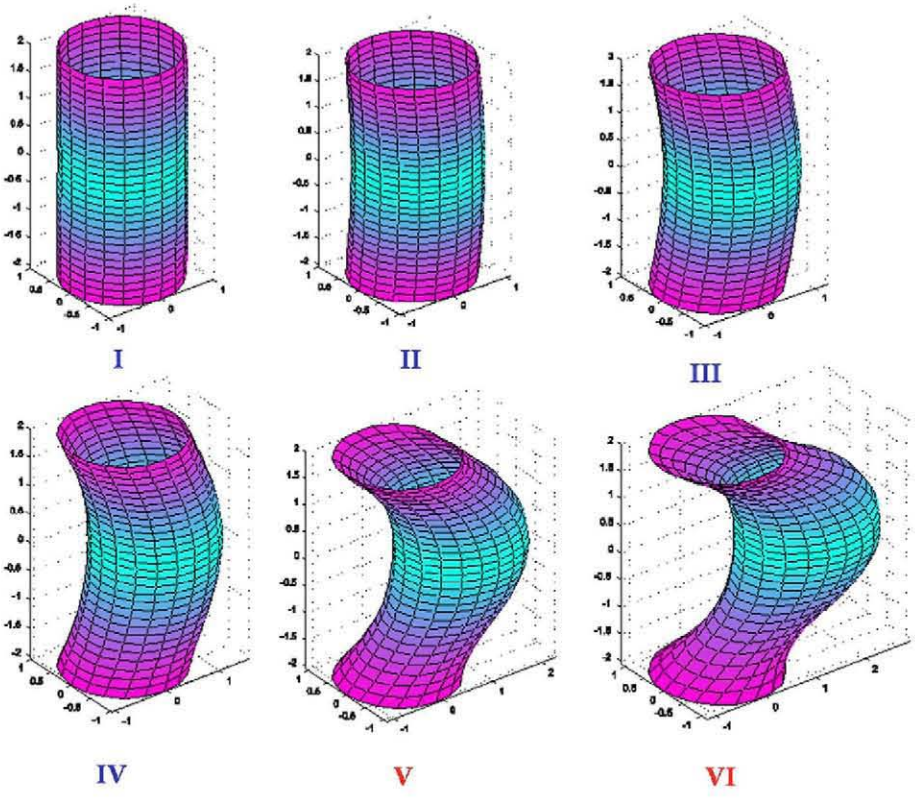

Fig. 9. Evolution of the equilibrium shapes of a cylindrical liquid bridge for the C-mode with $\Lambda = 1.9$ along the main branch of solution for $e = 0.1$. Shapes I to IV are stable and V and VI are unstable. Note that although the scale is from -2 to 2, the liquid bridge lays from -1.9 to 1.9.

where $W_0(\Lambda)$ is given by Eq. (25) and ϕ_{101} and ϕ_{120} are given in Perales et al. (1990). This relationship was sketched in Fig. 4. Thus, the effect of eccentricity for amphora mode does not change the character of the destabilization, as happened for C-mode, being due to a subcritical bifurcation point as happened for $e = 0$.

With the numerical method we have recovered the stability threshold for $e = 0$, and we have analyzed the dependence of this threshold on the eccentricity and the angular speed. Fig. 10 shows the variation of the stability threshold for increasing eccentricity. The line for $e = 0$ corresponds to the threshold represented in Fig. 2. As we can see in Fig. 10 an increase of the eccentricity decreases the stability region. The behavior of the stability threshold is different for lower values of the slenderness.

Fig. 11 compares the variation of W with e for both numerical and analytical results from Eq. (26) for $\Lambda = 2.9$ (marked with dashed line in Fig. 10). These results agree very well for $e \ll 1$ and the disagreement between analytical and numerical results increases as the eccentricity increases. The evolution of W with e for different values of Λ is shown in Fig. 12. As we can see in this figure, the effect of slenderness in the stability is similar to that for $e = 0$, that is, the increase of Λ decreases the stability region. This figure also shows that the eccentricity becomes less important for long liquid columns. The reason is that the stability limit tends to $W = 0$ for $\Lambda = \pi$ (see Fig. 2), so all the stability lines have to tend to this point.

The analytical behavior described by Eq. (25) is better recovered for higher values of the slenderness.

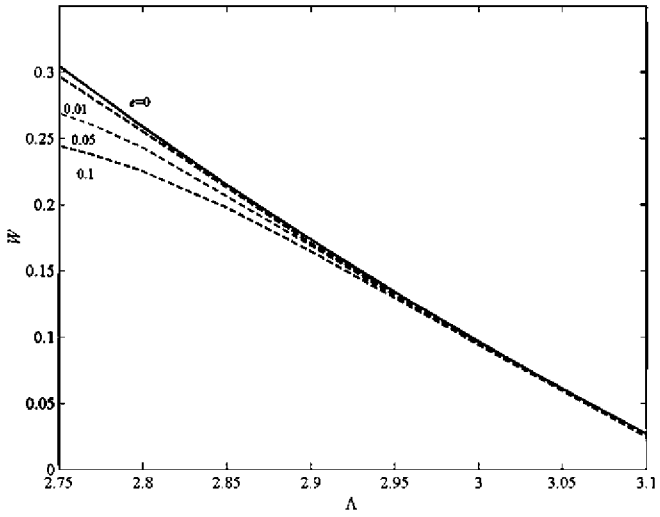

Fig. 10. Effect of the eccentricity on the threshold stability for amphora mode.

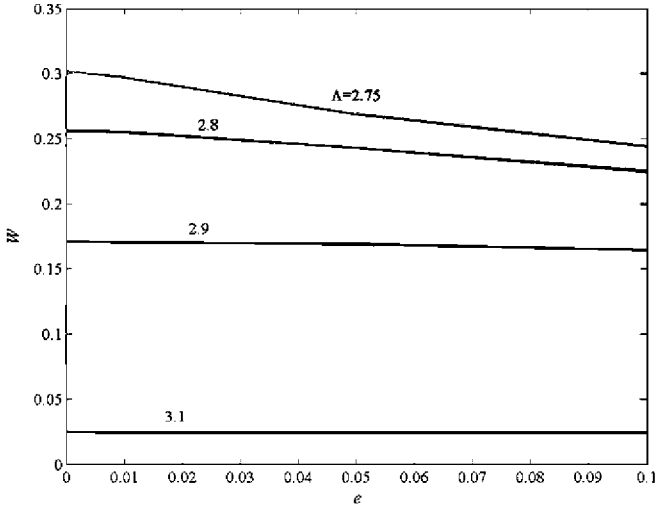

Fig. 12. Effect of the slenderness on the threshold stability for the amphora mode.

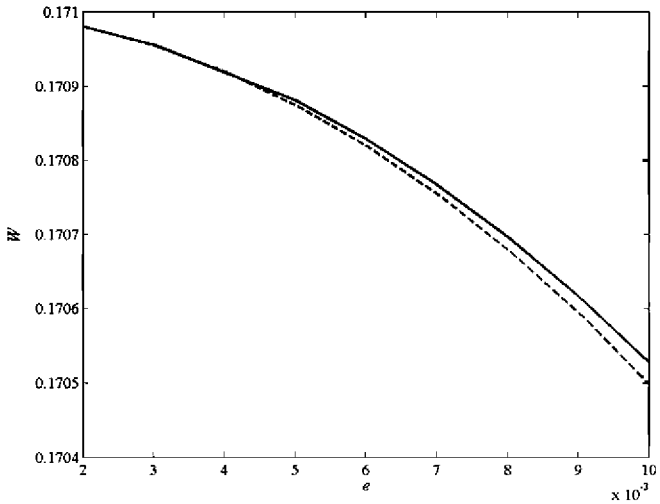

Fig. 11. Comparison between the numerical (solid line) and the analytical results (dashed line) for the amphora mode ($\Lambda = 2.9$).

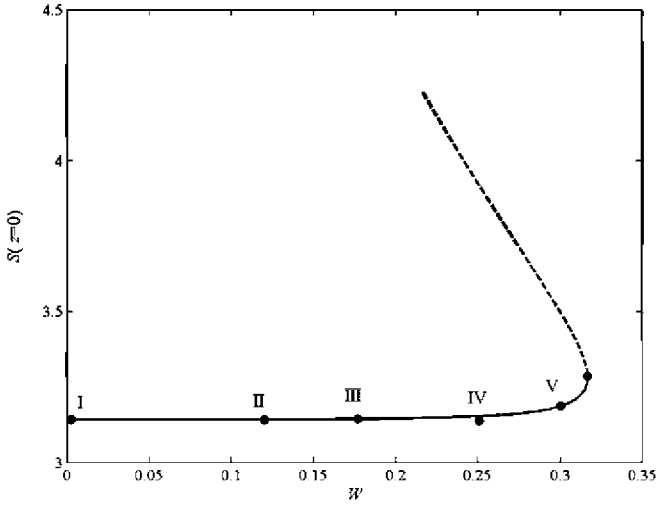

Fig. 13. Bifurcation diagram for the values of the parameters of the TEXUS-23 experiment ($\Lambda = 2.5$ and $e = 0.067$, C-mode).

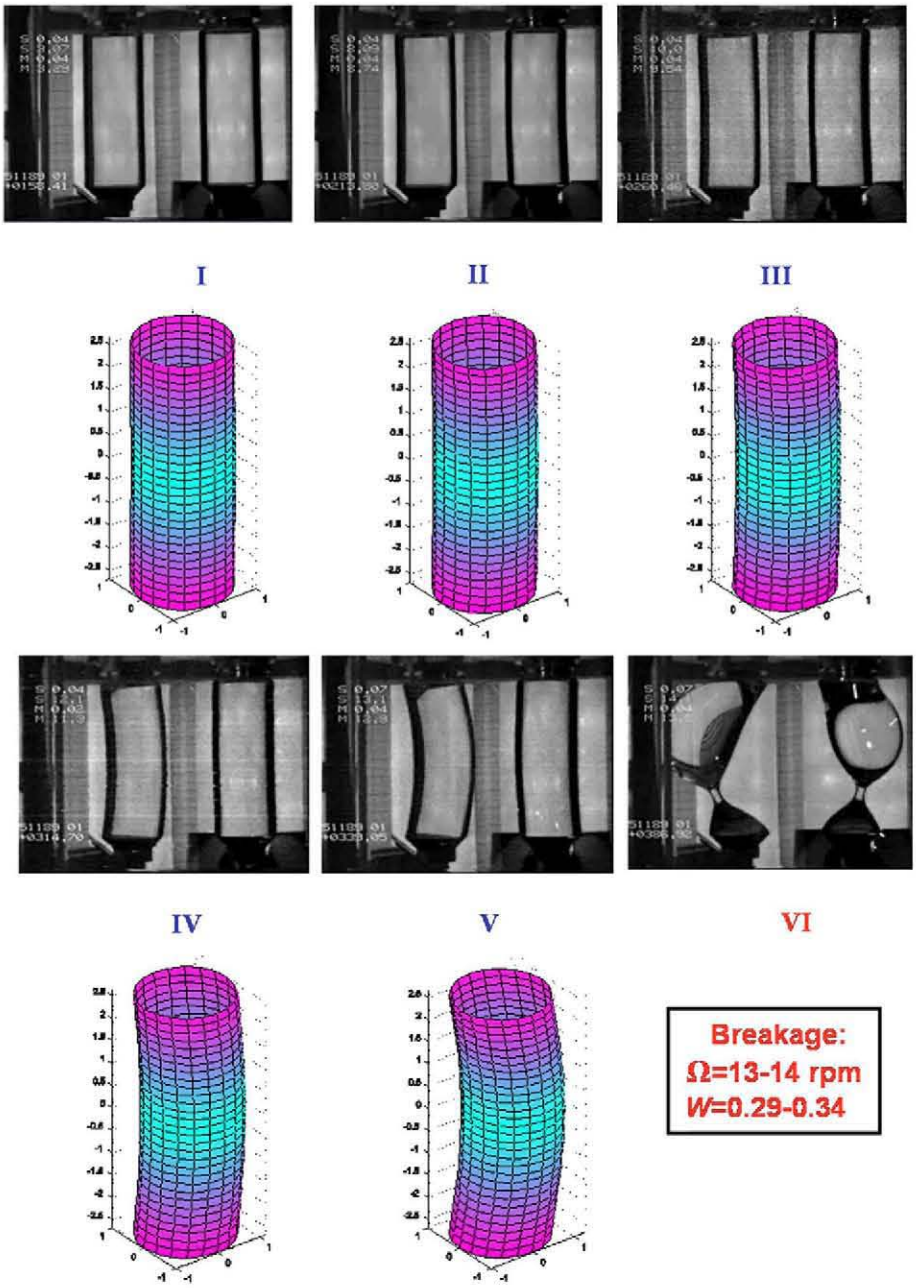

Fig. 14. Comparison of the equilibrium shapes of a cylindrical liquid for the numerical method and the TEXUS-23 experiment.

No bifurcation diagrams and equilibrium shapes are shown for this mode because there is not a substantial change of the character of the destabilization as happened for the C-mode, and no deformation of the liquid bridge is appreciated for the stable shapes.

5. Comparison with experimental results for C-mode

The experiment TEXUS-23 (Sanz et al., 1992) showed the deformation and final breakage of a liquid bridge of slenderness $\Lambda = 2.5$ subjected to an increasing angular speed around an eccentric axis ($e = 0.067$). This case was indicated in Fig. 5. In the experiment the breakage of the liquid bridge happened for a value of the angular speed between 13 and14 rpm, which corresponds to a Weber number between 0.29 and 0.34.

With the numerical method we have recovered the evolution of the liquid bridge and we have compared it with the experimental results. Fig. 13 shows the bifurcation diagram. The turning point occurs for $W = 0.317$, which is in the range of experimental values where the breakage of the bridge happens. Equilibrium shapes for points I to VI marked in Fig. 13 are represented in Fig. 14 and compared with the shapes of the bridge obtained in the experiment for the same values of the parameters. The images show two different views of the liquid bridge. As we can see, the numerical method recovers the deformation of the liquid bridge until the breakage.

6. Conclusions

The stability limits of liquid bridges rotating around an eccentric axis are calculated numerically and compared with the analytical results of Perales et al. (1990) (only valid for small eccentricity) recovering the same behavior for both amphora and C-modes. The numerical method is used to find stable and unstable shapes and to determine the dependence of the stability threshold on the slenderness and eccentricity, being this analysis not only restricted to small eccentricity as happened for the analytical study.

For both amphora and C-modes, the analysis shows that the stability region decreases, that is, overpassing of the stability threshold occurs at lower values of the angular speed, as slenderness or eccentricity increase.

For the C-mode, numerical results have also been compared with the results of an experiment aboard TEXUS-23 (Sanz et al., 1992) recovering the stability limit and the equilibrium shapes.

References

Keller, H.B. Lectures on Numerical Methods in Bifurcation Problems. Springer Verlag, Berlin, 1987.

Laverón-Simavilla, A., Checa, E. Effect of a lateral gravitational field on the non-axisymmetric equilibrium shapes of liquid bridges held between eccentric disks and of volumes equal to those of cylinders. Phys. Fluids 9, 817, 1997.

Laverón-Simavilla, A., Perales, J.M. Equilibrium shapes of nonaxisymmetric liquid bridges of arbitrary volume in gravitational fields and their potential energy. Phys. Fluids 7, 1204, 1995.

Meseguer, J., Sanz, A. Numerical and experimental study of the dynamics of axisymmetric slender liquid bridges. J. Fluid Mech. 153, 83, 1985.

Perales, J.M., Sanz, A., Rivas, D. Eccentric Rotation of a Liquid Bridge. Appl. Microgravity Tech. II 4, 193–197, 1990.

Sanz, A., Perales, J.M., Rivas, D., Rotational instability of a long liquid column. ESA SP-1132, vol. 2, pp. 8–21, 1992.

Vega, J.M., Perales, J.M., Almost cylindrical isorotating liquid bridges for small bond number. ESA SP-191, ESA, Paris, pp. 247–252, 1983.